Solid-State Photochemistry and Structure of *trans*-$(Et_3P)_2Ni(N_3)_2$: Photodeposition of Nickel

Anna Becalska, Raymond J. Batchelor, Frederick W. B. Einstein,* Ross H. Hill,* and Bentley J. Palmer

Department of Chemistry, Simon Fraser University, Burnaby, British Columbia, Canada, V5A 1S6

Received December 18, 1991

The photochemistry and stereochemistry of *trans*-$(Et_3P)_2Ni(N_3)_2$ have been investigated in the solid state. A single-crystal X-ray diffraction study of *trans*-$(Et_3P)_2Ni(N_3)_2$ shows that it crystallizes in the orthorhombic space group $Pbc2_1$ with a = 7.7011 (11) Å, b = 15.7112 (22) Å, c = 16.7813 (13) Å, and Z = 4 at 296 K (R_F = 0.030 for 1231 data, $I_o \geq 2.5\sigma(I_o)$; N_{var} = 132). The mechanism of this photoreaction has been studied at room temperature, 77 K, and 20 K. Photolysis into the d-d absorption resulted in the formation of ion-paired $[(Et_3P)_2Ni(N_3)]^+[N_3]^-$. Recoordination was achieved with UV ($\lambda > 310$ nm) photolysis. Excitation of the charge-transfer bands of *trans*-$(Et_3P)_2Ni(N_3)_2$ resulted in the formation of a species containing both bridging and terminal azide groups, $[(Et_3P)Ni(N_3)_2]_2$. Prolonged photolysis of the surface resulted in the loss of all ligands from the nickel. Analysis of the resultant film by Auger spectroscopy showed the production of nickel covered by a NiO layer and established the loss of all PEt_3 and nitrogen from the surface.

Introduction

The deposition of films of metals, metal oxides, and metal nitrides on surfaces has attracted a great deal of interest recently due to their importance in the semiconductor industry. Several methods of deposition have been used, including plasma techniques, chemical vapor deposition, and photochemical deposition.[1,2] Each method has advantages; the latter two have the advantage of low process temperatures. Additionally, the photochemical methods allow for beam-directed deposition of the desired film, simplifying the overall process methodology.[3]

In spite of the apparent low temperatures which should be possible for photochemical methods, the deposition process in many systems is not truly a photochemical process but a photon-energized thermal process. Although, an initial photon may lead to facile loss of a ligand and cause the molecule to adhere to the substrate, further decomposition is the result of thermolysis of the surface-bound species.[4,5] If the surface reactions could be induced in a true photochemical process, then the local-process temperature would also be reduced. Such low temperatures would be advantageous in the fabrication of multilevel VLSI devices. There is, however, little known about the photochemistry of surface-bound complexes. We have initiated[6] a study of films on surfaces with the goal of identifying facile photochemical reactions which may be induced at low temperatures.

In this study we have chosen to observe $(Et_3P)_2Ni(N_3)_2$ for a number of reasons. The complex is nonvolatile, allowing study in vacuum. The azido group is known to be photosensitive and may ultimately decompose to yield either the metal or metal nitride. It should be noted that both loss of N_2 from coordinated azide ligand and loss of the azide ligand as a radical have been observed to be induced photochemically in the solution phase.[7] The photochemistry of a related Ni(II) complex was found to be consistent with both of these processes.[8] The azido group is an intense chromophore in the IR region, allowing us to study lower surface coverages than were possible in our previous study.[6] Last, it should be noted that the free ligands, $N_3^\bullet$ and PEt_3, should be readily lost from the surface. This would leave metallic nickel, which is used as part of a contact mixture for n-type ohmic contacts in GaAs devices.[9] In order to interpret the photochemistry, the initial geometry of $(Et_3P)_2Ni(N_3)_2$ was determined.

Experimental Section

The CaF_2 crystals were obtained from Wilmad Glass Co. Inc. The Si(111) wafers were obtained from Pacific Microelectronics Center. The wafers were p-type silicon with tolerances and specifications as per SEMI Standard M1.1.STD.5. The wafers were cut to the approximate dimensions of 1 cm × 1.5 cm in-house. Sodium [1-^{15}N]azide was obtained from Cambridge Isotopes and was 99 atom % ^{15}N enriched in the 1-position.

The FTIR spectra were obtained with 4-cm^{-1} resolution using a BOMEM Michelson 120 FTIR spectrophotometer. The samples were held in either a CaF_2-faced cell (glasses) or a high-conductivity copper sample mount within a CaF_2-faced vacuum dewar. Experiments at 77 K were done by using liquid N_2 coolant in the vacuum dewar. Experiments at 20 K were performed using a CTI-Cryogenics Model 22 cryocooler and a 350R compressor system equipped with a Lake Shore Cryotronics DRC 80C temperature controller. The temperature was monitored with a Lake Shore Cryotronics silicon diode sensor (DT500DRC). The optical spectra were recorded with a Cary 17 spectrophotometer.

The photolysis beam was a 100-W high-pressure Hg lamp in an Oriel housing equipped with condenser lenses and filtered through a 10-cm water filter with Pyrex optics. This combination resulted in primarily LMCT excitation. In some experiments a band-pass filter ($\lambda > 420$ nm pass), interposed between the lamp and the sample, resulted in LF excitation.

X-ray photoelectron spectra were obtained using a PHI double-pass CMA at 0.85-eV resolution at the Surface Physics Laboratory, Department of Physics, Simon Fraser University.

Crystal Structure of *trans*-$(Et_3P)_2Ni(N_3)_2$. A deep red air-stable crystal was mounted on a Pyrex filament and thinly coated with epoxy resin. Intensity data (Mo Kα graphite monochromator) were collected with an Enraf-Nonius CAD-4F diffractometer. The unit cell was determined from 25 well-centered reflections ($30° \leq 2\theta \leq 40°$). The intensities of two standard reflections were measured every 1.3 h of acquisition time and declined systematically by 14% during the course of data acquisition. Data measured: $\pm h,\pm k,\pm l$, $4° \leq 2\theta \leq 20°$; hkl, $4° \leq 2\theta \leq 50°$. The data were corrected analytically for absorption.[10] Calculated and

(1) Almond, M. J.; Rice, D. A.; Yates, C. A. *Chem. Br.* **1988**, 1130.
(2) Singmaster, K. A.; Houle, F. A.; Wilson, R. J. *Appl. Phys. Lett.* **1988**, *53*, 1048.
(3) Gilgen, H. H.; Cacouris, T.; Shaw, P. S.; Krchnavek, R. R.; Osgood, R. M. *Appl. Phys. B* **1987**, *42*, 55.
(4) Gluck, N. S.; Ying, Z.; Bartosch, C. E.; Ho, W. *J. Chem. Phys.* **1987**, *86*, 4957.
(5) Herman, I. P. *Chem. Rev.* **1989**, *89*, 1323.
(6) Palmer, B. J.; Becalska, A.; Hill, R. H. *J. Photochem. Photobiol. A: Chem.* **1991**, *57*, 457. Palmer, B. J.; Becalska, A.; Hader, R.; Hill, R. H. *Polyhedron* **1991**, *8*, 877.
(7) Reed, J. L.; Wang, F.; Basolo, F. *J. Am. Chem. Soc.* **1972**, *94*, 7173. Bartocci, C.; Scandola, F. *J. Chem. Soc., Chem. Commun.* **1970**, 531. Endicott, J. F.; Hoffman, M. Z.; Beres, L. S. *J. Phys. Chem.* **1970**, *74*, 1021. See also references contained in ref 8.
(8) Ngai, R.; Wang, Y.-H. L.; Reed. J. L. *Inorg. Chem.* **1985**, *24*, 3802.
(9) Woodall, J. M. *AIP Conf. Proc.* **1986**, *138*, 223.
(10) Demeulenaer, J.; Tompa, H. *Acta Crystallogr.* **1965**, *19*, 1014.

0020-1669/92/1331-3118$03.00/0

Table I. Crystallographic Data for the Structure Determination of $Ni(PEt_3)_2(N_3)_2$ (1)

formula	$NiP_2N_6C_{12}H_{30}$	Z	4
fw	379.06	ρ_c, g cm^{-3}	1.240
cryst syst	orthorhombic	λ(Mo Kα_1), Å	0.709 30
space group[a]	$Pbc2_1$	μ(Mo Kα), cm^{-1}	11.2
a, Å	7.7011 (11)	min–max 2θ, deg	4–50
b, Å	15.7112 (22)	transm	0.758–0.864
c, Å	16.7813 (13)	R_F[b]	0.030
V, Å^3	2030.4	R_wF[c]	0.036

[a] General equivalent positions: x, y, z; $-x, y + {}^1/_2, z$; $x, -y + {}^1/_2, z + {}^1/_2$; $-x, -y, z + {}^1/_2$. [b] $R_F = \sum||F_o| - |F_c||/\sum|F_o|$, for reflections having $I_o \geq 2.5\sigma(I_o)$. [c] $R_{wF} = [\sum(w(|F_o| - |F_c|)/\sum(wF_o^2)]^{1/2}$, for reflections having $I_o \geq 2.5\sigma(I_o)$; $w = [\sigma(F_o)^2 + 0.0004F_o^2]^{-1}$.

measured ψ-scan intensity profiles were compared and showed excellent agreement. Data reduction included interpolated intensity scale variation and Lorentz and polarization corrections.

The symmetry and systematic conditions of the intensity-weighted reciprocal lattice showed the crystal to belong to the orthorhombic system with possible space groups being *Pbcm* and $Pbc2_1$ ($R_{int} = 0.008$). The structure was solved in $Pbc2_1$ after attempts in *Pbcm* were unfruitful. Analysis of the Bijvoet differences rigorously confirmed the crystal class of *mm*2 and, hence, also supported the assignment of the space group. In addition, the Bijvoet differences indicate that the refined model corresponds to the correct polarity. A total of 93 out of 109 Bijvoet differences showed the same sense in F_o as in F_c. The 50 most significant differences (ranging in $|F_c^+ - F_c^-|/\sigma(F_o)$ from 25 down to 3.4) all showed the same sense in F_o as in F_c.

Hydrogen atoms were placed in calculated positions and assigned isotropic thermal parameters initially 10% larger than those for the corresponding carbon atoms. The coordinates of the hydrogen atoms were linked with those of their respective carbon atoms. A single least-squares parameter was refined for the isotropic thermal motion of the hydrogen atoms of the methyl groups and another for those of the methylene groups. A constrained set of anisotropic thermal parameters was refined for each pair of non-hydrogen atoms related by the local pseudo-inversion at Ni, since an independent refinement indicated that they were similar. The origin was fixed by restraining the sum of the z shifts. A weighting scheme based on counting statistics was applied such that $\langle w(|F_o| - |F_c|)^2 \rangle$ was nearly constant as a function of both $|F_o|$ and $((\sin\theta)/\lambda)^2$. The final full-matrix least-squares refinement of 132 parameters for 1231 data ($I_o \geq 2.5\sigma(I_o)$) converged at $R_F = 0.030$.

Complex scattering factors for neutral atoms[11] were used in the calculation of structure factors. The programs used for data reduction, structure solution and initial refinement, and Bijvoet pair analysis were from the NRCVAX crystal structure system.[12] The program suite CRYSTALS[13] was employed in the final refinement. All computations were carried out on a MicroVAX-II computer. Crystallographic data are summarized in Table I. The final positional and isotropic or equivalent isotropic thermal parameters for the non-hydrogen atoms are given in Table II. Additional experimental details and coordinates and temperature factors for the hydrogen atoms, as well as the anisotropic temperature factors, a list of observed and calculated structure factors, and details of the Bijvoet analysis are deposited as supplementary material.

Preparation of *trans*-$(Et_3P)_2Ni(N_3)_2$. The procedure followed was a modification of that used by Bowman and Dori.[14] We give the details below for the ^{15}N-labeled derivative.

To a solution containing *trans*-$(Et_3P)_2Ni(Cl)_2$ (0.04 g) in acetone (20 mL) was added solid [1-^{15}N]NaN_3 (0.026 g). After the mixture was stirred for 24 h and filtered, the solvent was removed under reduced pressure. The solid was extracted with hexane, which was then removed to yield [$^{15}N_2$]-*trans*-$(Et_3P)_2Ni(N_3)_2$, 0.035 g.

Photolysis of Complexes in a (1,2-Epoxyethyl)benzene Glass. A sample of *trans*-$(Et_3P)_2Ni(N_3)_2$ was dissolved in 1,2-epoxyethylbenzene and loaded into a CaF_2-faced cell. The sample was cooled to 77 K and the FTIR spectrum obtained. The sample was then irradiated with UV light for 20, 50, 87, 127, and 147 min. No change was observed in the FTIR spectra in the region of the antisymmetric azide stretch.

Calibration of Absorption on a Surface. A stock solution of *trans*-$(Et_3P)_2Ni(N_3)_2$ (0.0028 g) was prepared in CH_2Cl_2 (3.0 mL). A drop (0.0031 mL) of this solution was then deposited on the surface of a Si wafer and allowed to evaporate, and the FTIR spectrum was obtained. The area of the drop was found to be 0.5 cm^2. This corresponds to a coverage of 0.9 molecule/Å^2. This process was repeated several times.

Photolysis of Complexes on Si Surfaces. For photolysis, a Si surface was prepared with *trans*-$(Et_3P)_2Ni(N_3)_2$ as above and transferred to the vacuum dewar. This was then photolyzed for 15, 35, 55, 90, and 240 min with a filter (band-pass $\lambda > 420$ nm) interposed between the sample and light source. Further photolysis was conducted with only a H_2O filter (10 cm in Pyrex optics) for 3, 8, 35, 72, 102, and 1182 min. Spectral changes are summarized in Figure 3. In some cases the film was prepared by spin-coating the nickel complex, from a CH_2Cl_2 solution, onto the Si chip. This procedure gave rise to a more uniform film but had no effect on the observed photochemistry. Similar experiments were done at 77 and 20 K.

Table II. Fractional Coordinates (×10^4) and Equivalent Isotropic Temperature Factors (Å^2 × 10^4) for the Non-Hydrogen Atoms of $Ni(PEt_3)_2(N_3)_2$ (1)

atom	x/a	y/b	z/c[a]	U_{eq}[b]
Ni	7635.3 (8)	6201.6 (4)	9995 (2)	522
P(1)	9151 (2)	6818 (1)	10966 (2)	573
P(2)	6100 (2)	5593 (1)	9027 (2)	573
N(1)	9549 (7)	6199 (4)	9307 (4)	798
N(2)	9881 (8)	6662 (5)	8794 (4)	878
N(3)	10319 (13)	7066 (8)	8292 (7)	1485
N(4)	5713 (7)	6221 (4)	10673 (4)	798
N(5)	5338 (8)	5708 (5)	11146 (5)	878
N(6)	4881 (14)	5235 (8)	11597 (6)	1485
C(1)	11363 (8)	7141 (5)	10728 (4)	789
C(2)	12339 (8)	7641 (7)	11354 (6)	1036
C(3)	8084 (9)	7769 (5)	11326 (5)	784
C(4)	7689 (11)	8389 (5)	10691 (7)	1152
C(5)	9323 (10)	6125 (4)	11845 (5)	787
C(6)	10020 (14)	5257 (5)	11643 (6)	1122
C(7)	3916 (7)	5247 (5)	9299 (4)	789
C(8)	2904 (9)	4790 (6)	8648 (6)	1036
C(9)	7187 (8)	4660 (5)	8634 (5)	784
C(10)	7555 (10)	3994 (5)	9262 (7)	1152
C(11)	5824 (10)	6284 (4)	8180 (4)	787
C(12)	5157 (12)	7158 (5)	8378 (6)	1122

[a] The origin was fixed by restraining $\sum(z/c)$ to be invariant. [b] U_{eq} is the cube root of the product of the principal components of the thermal ellipsoid.

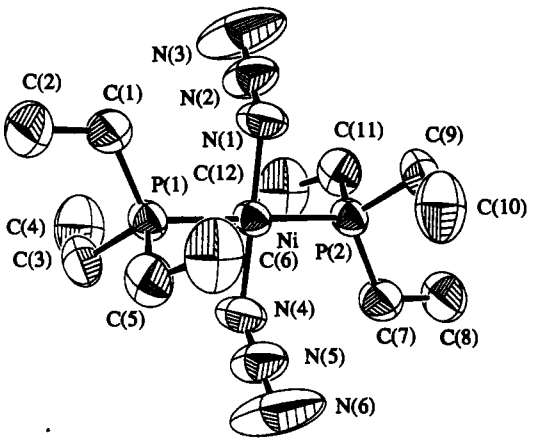

Figure 1. Molecular structure of *trans*-$(Et_3P)_2Ni(N_3)_2$ (hydrogen atoms excluded; 50% enclosure thermal ellipsoids).

Results and Discussion

Solid-State Structure of *trans*-$(Et_3P)_2Ni(N_3)_2$. The molecular structure of *trans*-$(Et_3P)_2Ni(N_3)_2$ is shown in Figure 1. Selected intramolecular distances and angles are listed in Table III. Selected bond torsion angles are listed in Table IV. The molecular conformation shows relatively small deviations from

(11) *International Tables for X-ray Crystallography*; Kynoch Press: Birmingham, England, 1975; Vol. IV, p 99.
(12) Gabe, E. J.; LePage, Y.; Charland, J.-P.; Lee, F. L.; White, P. S. NRCVAX An Interactive Program System for Structure Analysis. *J. Appl. Cryst.* **1989**, *22*, 384.
(13) Watkin, D. J.; Carruthers, J. R.; Betteridge, P. W. *CRYSTALS*; Chemical Crystallography Laboratory, University of Oxford: Oxford, England, 1984.
(14) Bowman, K.; Dori, Z. *Inorg. Chem.* **1970**, *9*, 395.

Table III. Selected Bond Distances and Angles for $Ni(PEt_3)_2(N_3)_2$ (**1**)

	Distances (Å)		
Ni–P(1)	2.226 (2)	Ni–N(1)	1.872 (5)
Ni–P(2)	2.225 (2)	Ni–N(4)	1.867 (6)
P(1)–C(1)	1.822 (6)	P(2)–C(7)	1.826 (6)
P(1)–C(3)	1.809 (7)	P(2)–C(9)	1.813 (7)
P(1)–C(5)	1.838 (7)	P(2)–C(11)	1.801 (6)
N(1)–N(2)	1.155 (8)	N(4)–N(5)	1.169 (8)
N(2)–N(3)	1.107 (10)	N(5)–N(6)	1.117 (10)
C(1)–C(2)	1.512 (10)	C(7)–C(8)	1.522 (10)
C(3)–C(4)	1.476 (12)	C(9)–C(10)	1.512 (12)
C(5)–C(6)	1.504 (11)	C(11)–C(12)	1.503 (10)
	Angles (deg)		
P(2)–Ni–P(1)	179.48 (7)	N(4)–Ni–P(1)	87.8 (2)
N(1)–Ni–P(1)	92.3 (2)	N(4)–Ni–P(2)	91.8 (2)
N(1)–Ni–P(2)	88.1 (2)	N(4)–Ni–N(1)	179.0 (3)
C(1)–P(1)–Ni	116.8 (3)	C(5)–P(1)–Ni	111.6 (3)
C(3)–P(1)–Ni	111.4 (3)	C(5)–P(1)–C(1)	105.9 (4)
C(3)–P(1)–C(1)	105.5 (4)	C(5)–P(1)–C(3)	104.7 (4)
C(7)–P(2)–Ni	115.8 (3)	C(11)–P(2)–Ni	112.3 (3)
C(9)–P(2)–Ni	111.6 (3)	C(11)–P(2)–C(7)	105.6 (4)
C(9)–P(2)–C(7)	106.0 (4)	C(11)–P(2)–C(9)	104.8 (4)
N(2)–N(1)–Ni	129.2 (6)	N(5)–N(4)–Ni	126.8 (6)
N(3)–N(2)–N(1)	174.1 (12)	N(6)–N(5)–N(4)	175.9 (11)
C(2)–C(1)–P(1)	117.2 (6)	C(8)–C(7)–P(2)	115.6 (6)
C(4)–C(3)–P(1)	113.4 (7)	C(10)–C(9)–P(2)	113.1 (6)
C(6)–C(5)–P(1)	112.5 (7)	C(12)–C(11)–P(2)	114.6 (7)

local (noncrystallographic) inversion symmetry centered at Ni. The atoms Ni, P(1), P(2), N(1), and N(4) are coplanar within our errors. The torsion angle between the vectors defined by N(1)–N(3) and N(4)–N(6) about the axis defined by N(1)–N(4) is 172.5 (6)°.

The Ni–N bond lengths (1.872 (5), 1.867 (6) Å) are shorter than those found in five- or six-coordinate Ni(II) complexes for nonbridging azide ligands (1.95 (1)–2.11 (1) Å)[15-18] or in a tetrahedrally coordinated Ni^{I} complex[19] (2.018 (8)). The Ni–N–N bond angles (129.2 (6), 126.8 (6)°) are comparable to those for the above-mentioned structures (128.1 (9)[19]–138.4 (2)° [15]). In contrast, terminally bound isothiocyanate ligands in similar square-planar Ni^{II} complexes generally display Ni–N–C bond angles closer to 180° and shorter Ni–N bonds (cf. 176.9 (3)° and 1.826 (3) Å[20]). The dimensions of the N–N–N group are comparable with those of previous azide structures. While the bond lengths for N(2)–N(3) and N(5)–N(6) appear shorter than N(1)–N(2) and N(4)–N(5), we do not consider these differences to be significant in light of the errors introduced by the large thermal motion of these atoms, which results in the determined distances being systematically shorter than the actual values.

The molecular packing is approximately hcp with the pseudo-hexagonal axis along *c*. There are no intermolecular distances less than the sums of the appropriate pairs of van der Waals radii.

Spectroscopic Data for the Complexes. The electronic spectra of *trans*-$(Et_3P)_2Ni(N_3)_2$ and related complexes[21] are reported in Table V. The lowest energy band is associated with d–d transitions. We expect three transitions in this region.[22,23] The lowest energy expected transition, $d_{z^2} \rightarrow d_{x^2-y^2}$, is not resolved from the next highest energy transitions, $d_{xz},d_{yz} \rightarrow d_{x^2-y^2}$. The remaining d–d transition, $d_{xy} \rightarrow d_{x^2-y^2}$, is expected at slightly higher energy and results in a distinct asymmetry of the d–d absorption band. The next resolved absorption band is associated with the $N_3^-(\pi) \rightarrow d_{x^2-y^2}$ LMCT transition. These proposed assignments are based on the assignments presented for the halogen complexes, $(Me_3P)_2Ni(X)_2$ (X = Cl, Br, I).[22]

The first noteworthy feature is that the positions of the absorption maxima change only slightly upon changing from the nonpolar solvent benzene to a surface film. This is consistent with the noncoordinating nature of benzene and the lack of any significant interaction between molecules in the crystal structure. The comparison with other ligands is as expected. The high-energy LMCT band (or perhaps a 3d–4p transition) is between the positions observed for the Cl^- and Br^- derivatives, as expected from the optical electronegativities.[23] Similarly, the d–d transitions follow the same trend as expected from the spectrochemical series.[23]

The FTIR spectrum, in the region of the antisymmetric azide stretch, for different coverages of *trans*-$(Et_3P)_2Ni(N_3)_2$ on a Si surface is shown in Figure 2a. Note that little change in appearance is observed over the coverage range 0.8 to ~4 molecules/Å^2. The linear nature of the plot in Figure 2b indicates that there is no detectable thermal chemistry occurring upon deposition. It should also be noted that this invariance of the absorption spectra is consistent with the thickness of the film being utilized in this study. From the crystal structure we estimate the areal coverage of a molecule in the film to be 64 Å^2. This coverage is in the range required for technically useful films.[24] A total coverage of 1 molecule/Å^2 thus corresponds to 64 monolayers. In each of the photochemical experiments, the films studied are in excess of 60 monolayers thick, and the observed absorption is due to the *bulk* film. The interfacial layer, at either the silicon or the vacuum interface, is not making a significant contribution to the observed spectra. The silicon surface is not terminated by Si but rather by an oxide layer, the surface of which is thought to terminate in hydroxy groups.

The FTIR data for *trans*-$(Et_3P)_2Ni(N_3)_2$ and its ^{15}N-labeled derivatives are summarized in Table VI. The most intense peak is that associated with the antisymmetric azide stretch, which appears at 2041 cm^{-1}. This band shifts to lower energy in the *trans*-$(Et_3P)_2Ni(^{15}NN_2)_2$ derivative. The labeled complex is a mixture of $(Et_3P)_2Ni(^{15}N^{14}N_2)_2$, $(Et_3P)_2Ni(^{14}N_2{}^{15}N)_2$, and $(Et_3P)_2Ni(^{14}N_2{}^{15}N)(^{15}N^{14}N_2)$ in the ratio of 1:1:2. We observe the sum of the respective spectra, which results in a broadened antisymmetric stretch. Similar mixtures have been observed previously in monoazido compounds.[25]

Photochemistry of *trans*-$(Et_3P)_2Ni(N_3)_2$. Photolysis of *trans*-$(Et_3P)_2Ni(N_3)_2$ in (1,2-epoxyethyl)benzene glass at 77 K into either the charge-transfer or d–d transitions resulted in no change in the FTIR spectra. The photolysis time was such that if a reaction occurred with an efficiency comparable to that found on the surface, it would have been detectable.

Before describing the photochemistry in the film, it is worth considering how the film thickness affects the absorption. In the films studied here we can approximate the thickness of the film as 51 nm (calculated for 64 monolayers). Since this is less than the wavelength of light utilized (a range of 300–450 nm), the film will be irradiated evenly throughout. We should not see evidence of uneven irradiation causing reaction initially at the surface vacuum interface. This is consistent with what is described below.

The photochemistry described below was conducted at room temperature, 77 K, and 20 K. The only difference found as a

(15) Chaudhuri, P.; Guttmann, M.; Ventur, D.; Wieghardt, K.; Nuber, B.; Weiss, J. *J. Chem. Soc., Chem. Commun.* **1985**, 1618.
(16) Wagner, F.; Mocella, M. T.; D'Aniello, M. J., Jr.; Wang, A. H.-J.; Barefield, E. K. *J. Am. Chem. Soc.* **1974**, *96*, 2625.
(17) D'Aniello, M. J., Jr.; Mocella, M. T.; Wagner, F.; Barefield, E. K.; Paul, I. C. *J. Am. Chem. Soc.* **1975**, *97*, 192.
(18) Paap, F.; Driessen, W. L.; Reedijk, J.; Kojic-Prodic, B.; Spek, A. L. *Inorg. Chim. Acta* **1985**, *104*, 55.
(19) Enemark, J. H. *Inorg. Chem.* **1971**, *10*, 1952.
(20) Foxman, B. M.; Goldberg, P. L.; Mazurek, H. *Inorg. Chem.* **1981**, *20*, 4368.
(21) Coussmaker, C. R. C.; Hutchinson, M. H.; Mellor, J. R.; Sutton, L. E.; Venanzi, L. M. *J. Chem. Soc.* **1961**, 2705.
(22) Merle, A.; Dartiguenave, M.; Dartiguenave, Y. *J. Mol. Struct.* **1972**, *13*, 413.
(23) Ferraudi, G. J. *Elements of Inorganic Photochemistry*; Wiley: New York, 1988.
(24) Rand, M. J. *J. Electrochem. Soc.* **1973**, *120*, 686.
(25) Kurtz, D. M., Jr.; Shriver, D. F.; Klotz, I. M. *J. Am. Chem. Soc.* **1976**, *98*, 5033. Pate, J. E.; Thamann, T. J.; Solomon, E. I. *Spectrochim. Acta* **1986**, *42A*, 313.

Table IV. Selected Intramolecular Torsion Angles (deg) for $Ni(PEt_3)_2(N_3)_2$ (1)

N(1)–Ni–P(1)–C(1)	4.9 (3)	N(4)–Ni–P(2)–C(7)	−8.1 (3)	Ni–P(1)–C(5)–C(6)	53.4 (4)	Ni–P(2)–C(11)–C(12)	−50.9 (4)
N(1)–Ni–P(1)–C(3)	126.3 (3)	N(4)–Ni–P(2)–C(9)	−129.4 (3)	Ni–P(1)–C(3)–C(4)	−54.6 (4)	Ni–P(2)–C(9)–C(10)	57.8 (4)
N(4)–Ni–P(1)–C(1)	−174.1 (3)	N(1)–Ni–P(2)–C(7)	172.9 (3)	C(5)–P(1)–C(1)–C(2)	−61.3 (5)	C(11)–P(2)–C(7)–C(8)	58.1 (5)
N(4)–Ni–P(1)–C(5)	63.9 (3)	N(1)–Ni–P(2)–C(11)	−65.7 (3)	C(1)–P(1)–C(3)–C(4)	73.1 (5)	C(7)–P(2)–C(9)–C(10)	−69.1 (5)
N(1)–Ni–P(1)–C(5)	−117.0 (3)	N(4)–Ni–P(2)–C(11)	113.3 (3)	C(3)–P(1)–C(1)–C(2)	49.4 (5)	C(9)–P(2)–C(7)–C(8)	−52.7 (5)
N(4)–Ni–P(1)–C(3)	−52.7 (3)	N(1)–Ni–P(2)–C(9)	51.6 (3)	C(5)–P(1)–C(3)–C(4)	−175.3 (7)	C(11)–P(2)–C(9)–C(10)	179.6 (7)
P(1)–Ni–N(1)–N(2)	−99.7 (5)	P(2)–Ni–N(4)–N(5)	93.6 (5)	C(1)–P(1)–C(5)–C(6)	−74.7 (5)	C(7)–P(2)–C(11)–C(12)	76.1 (5)
P(1)–Ni–N(4)–N(5)	−86.8 (5)	P(2)–Ni–N(1)–N(2)	79.9 (5)	C(3)–P(1)–C(5)–C(6)	174.1 (7)	C(9)–P(2)–C(11)–C(12)	−172.2 (7)
Ni–P(1)–C(1)–C(2)	173.8 (6)	Ni–P(2)–C(7)–C(8)	−176.9 (6)				

Table V. Optical Data for Relevant Complexes (in Benzene Unless Otherwise Noted)

complex	λ, nm (ε, M^{-1} cm^{-1}) LMCT	d–d
trans-$(Et_3P)_2Ni(N_3)_2$	364 (10 000)	476 (230)
trans-$(Et_3P)_2Ni(N_3)_2$[a]	360 (100)[b]	470 (2.5)[b]
trans-$(Et_3P)_2Ni(Cl)_2$	370 (14 200)	490 (450)
trans-$(Et_3P)_2Ni(Br)_2$	400 (6200)	542 (350)
trans-$(Et_3P)_2Ni(I)_2$	373 (4690), 459 (2900)	610 (485)

[a] Absorption spectrum recorded on a film deposited on a quartz surface. [b] Intensity data are an arbitrary scale and should be regarded with caution due to scattering.

Table VI. FTIR Spectral Data for Relevant Complexes on Si(111)

complex	$\nu_a(N_3)$, cm^{-1}	complex	$\nu_a(N_3)$, cm^{-1}
trans-$(Et_3P)_2Ni(N_3)_2$	2042	N_3^-	2124
$[^{15}N_2]$-*trans*-$(Et_3P)_2Ni(N_3)_2$	2029	$[1\text{-}^{15}N]N_3^-$	2117
$[(Et_3P)_2Ni(N_3)]^+$	2041	$[(Et_3P)Ni(N_3)_2]_2$	2074, 2023
$[^{15}N_2][(Et_3P)_2Ni(N_3)]^+$	2029	$[^{15}N_4][(Et_3P)\text{-}Ni(N_3)_2]_2$	2060, 2015

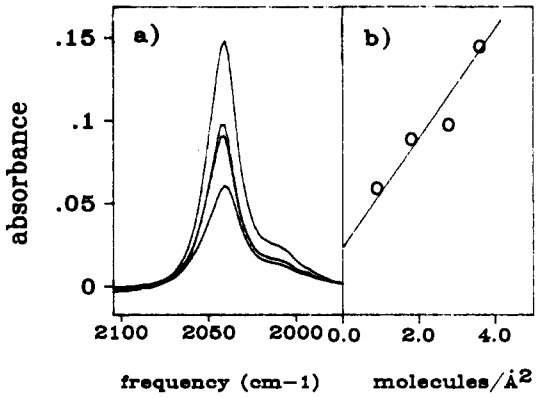

Figure 2. (a) FTIR spectra associated with 0.9, 1.8, 2.7, and 3.6 molecules of *trans*-$(Et_3P)_2Ni(N_3)_2/Å^2$ on a silicon surface. (b) Plot of absorbance of the antisymmetric N_3 stretch of *trans*-$(Et_3P)_2Ni(N_3)_2$ vs coverage (data from Figure 2a).

result of the temperature change was that the reaction was less efficient at lower temperatures. Photolysis of *trans*-$(Et_3P)_2Ni(N_3)_2$ on a surface was initially conducted with visible light and consequently results in d–d excitation. The spectral changes observed in the region of the antisymmetric azide stretch are shown in Figure 3a. Loss of the antisymmetric stretch of the azide groups is accompanied by the appearance and concomitant growth of a new absorption at 2124 cm^{-1}. This band is associated with a new azide chromophore, as demonstrated by a 7-cm^{-1} shift to lower energy upon ^{15}N labeling of the precursor complex. We associate this absorption with the free azide ion in the film. In order to confirm this, a mixture of *trans*-$(Et_3P)_2Ni(N_3)_2$ and NaN_3 was codeposited from acetone. Both the energy and bandwidth of the bands associated with N_3^- deposited in this way were indistinguishable from those of the band formed on photolysis. A similar result was found for the labeled derivative.

In order to determine the number of azide ligands lost as a result of d–d excitation, several samples were photolyzed exhaustively with LF excitation. The loss of absorption at 2042

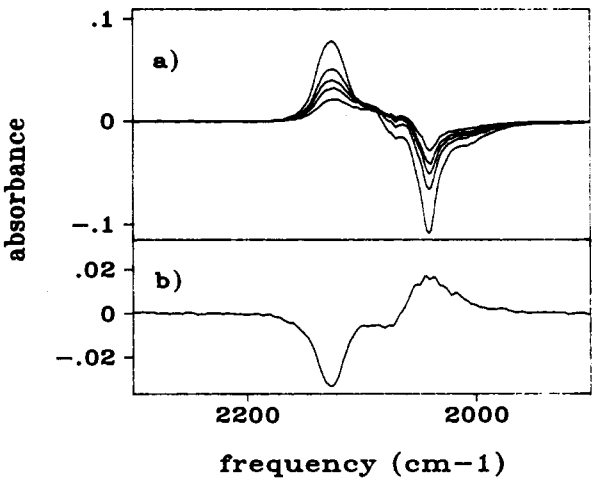

Figure 3. FTIR spectral changes associated with (a) photolysis (visible light) of a film of *trans*-$(Et_3P)_2Ni(N_3)_2$ on a silicon surface for 15, 35, 55, 90, and 240 min and (b) photolysis (ultraviolet light) of the resultant film for 3 min.

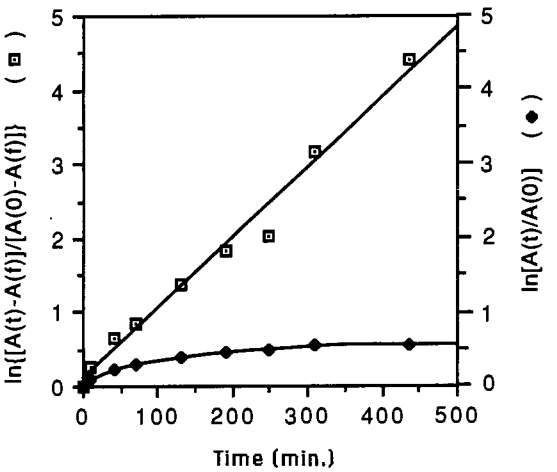

Figure 4. Plots of ln $[(A(t) - A(f))/(A(0) - A(f))]$ and ln $[A(t)/A(0)]$ vs photolysis time for the absorbance at 2042 cm^{-1}.

cm^{-1} never exceeded 50% of the original absorption independent of the initial film thickness used. Plots of ln $[(A(t) - A(f))/(A(0) - A(f))]$ vs photolysis time were linear if a final absorbance of 0.53 times the initial absorbance (Figure 4) was used. Plots of ln $[A(t)/A(0)]$ vs time were not linear (Figure 4). This behavior is indicative of the photoproduct absorbing in the same region as the starting complex (see Appendix for details). The remaining azide absorption is, hence, nearly degenerate with the absorption of the initial complex. The primary photoreaction is as given in eq 1.

$$\textit{trans}\text{-}(Et_3P)_2Ni(N_3)_2 \xrightarrow{h\nu\ (\lambda > 420\ nm)} (Et_3P)_2Ni(N_3)^+ + N_3^- \quad (1)$$

There is precedent for loss of coordinated azide upon d–d

excitation of $[Co(CN)_5N_3]^{3-}$.[26] We are aware of no example in the photochemistry of d^8 square planar complexes in which loss of azide ion upon d–d excitation has been demonstrated although loss of other anionic ligands are well documented.[27,28] It is interesting to note that the result of photolysis of *cis*-$(Ph_3P)_2Pt(N_3)_2$ has been interpreted in terms of sequential loss of N_3 radicals to form $Pt(PPh_3)_2$.[29] We see no evidence for a similar process here. The photochemistry of $(Me_3P)_2NiCl(N_3)$ has recently been studied in solution.[30] In this case, loss of N_2 upon exposure to light resulted in the ultimate formation of clusters through the intermediacy of a nickel nitrido species.

It is worth pointing out that no spectral changes consistent with either a trans to cis isomerism or a square planar to tetrahedral isomerism were observed. There is precedent for both of these reactions in solution phase.[29,31] Both of these are ruled out by the observation of unligated N_3^-.

Photolysis of surfaces containing $(Et_3P)_2Ni(N_3)^+$ and N_3^- with UV light resulted in the recoordination of N_3^- and regeneration of $(Et_3P)_2Ni(N_3)_2$. The spectral changes are shown in Figure 3b. The band due to $(Et_3P)_2Ni(N_3)_2$ is slightly broader than the band observed for a freshly deposited film consistent with some reorientation within the film. Consistent with this interpretation, the subsequent photochemistry is independent of initial conversion to $(Et_3P)_2Ni(N_3)^+$ and N_3^-. It should be noted that this photochemical recoordination reaction did not occur thermally. In the dark, films containing $(Et_3P)_2Ni(N_3)^+$ and N_3^- were stable over several hours.

UV photolysis of either freshly deposited *trans*-$(Et_3P)_2Ni(N_3)_2$ or a sample which had been through the above cycle resulted in loss of intensity at 2042 cm^{-1} and concomitant growth of two absorption bands at 2074 and 2023 cm^{-1}. The use of ^{15}N-labeled material resulted in the shift of each of these bands to lower energy (2060 and 2015 cm^{-1}, respectively). We assign these as due to the dimer, $[(Et_3P)Ni(N_3)_2]_2$.[32] The appearance of two well-separated bands in azide complexes is often indicative of both terminal and bridging azides. The isoelectronic molecule $[(Ph_3P)Pd(N_3)_2]_2$ has terminal and bridging azide absorptions at 2075 and 2027 cm^{-1}.[33] It is worth noting that the monomeric Pd complex, $(Ph_3P)_2Pd(N_3)_2$, has its antisymmetric azide stretch at 2035 cm^{-1}, similar in energy to *trans*-$(Et_3P)_2Ni(N_3)_2$ at 2042 cm^{-1}. This indicates that the IR spectra of analogous azide complexes of Ni and Pd are indeed similar. The reaction is shown in eq 2.

$$2\ \textit{trans}\text{-}(Et_3P)_2Ni(N_3)_2 \xrightarrow{h\nu\ (\lambda > 313\ nm)} [(Et_3P)Ni(N_3)_2]_2 + 2PEt_3 \quad (2)$$

The initial photoreaction is most reasonably ejection of a single PEt_3 ligand and formation of a three-coordinate Ni(II) species, $(PEt_3)Ni(N_3)_2$. This is followed by an associative reaction to form the observed azide-bridged dimer and PEt_3. It is notable that the thermal synthesis of $[(Ph_3P)Pd(N_3)_2]_2$ also occurs as a result of initial phosphine loss although in solution the intermediate is presumably solvated.[33] Photoinduced loss of PPh_3 from the related palladium complex $(Ph_3P)_2Pd(N_3)_2$ has been reported.[34]

Prolonged photolysis results in a gradual decrease in the intensity of absorptions associated with $[(Et_3P)Ni(N_3)_2]_2$ and the appearance of a weak absorption at 1995 cm^{-1}. This achieves a low steady-state intensity and eventually is lost, leaving no absorption in the azide region. The total integrated intensity of azide remaining at the point where the 1995-cm^{-1} band achieves its maximum intensity is 50% (at which point it accounts for less than 10% of the remaining azide). Assuming the same oscillator strength for all antisymmetric azide stretches, this indicates less than 50% of the Ni groups have direct bonding to an azide. Presumably, this indicates the formation of cluster sites. This process is probably accompanied by the formation of N_2; however, at no point is any species consistent with coordinated N_2 detectable by IR spectroscopy. Similarly, free N_2 trapped within the film is not observed.[35]

The absorption at 1995 cm^{-1} is at unusually low energy for a metal azide; however, ^{15}N labeling results in a shift of 9 cm^{-1} to lower energy. In view of the recent results[36] concerning free (i.e. non-ion-paired) N_3^- in a low-temperature matrix, we assign the 1995-cm^{-1} absorption to free N_3^-. The reported antisymmetric frequency for N_3^- in a N_2 matrix is 2003.5 cm^{-1}. This shifts to lower energy (by 10.5 cm^{-1}) in $^{14}N_2{}^{15}N^-$.[36] The formation of the unpaired N_3^- would be expected, as metallic nickel is formed and the positive charge is no longer localized on a single metal. Continued photolysis of the film at room temperature results in the observation of loss of intensity of absorptions due to both nitrogen-containing ligands and the original phosphine (C–H) modes. The only absorptions remaining are due to uncoordinated PEt_3.

The final films, resultant after prolonged photolysis, were removed and transferred to the X-ray photoelectron spectrometer. Analysis was then conducted by Auger spectroscopy and ESCA. The first apparent product on the surface is NiO. This is evident from the Ni and O peaks. The energy, shape, and relative intensity of the lines are all characteristic of NiO. Surprisingly, no signal due to P was observed, indicating that all P had been lost from the surface. This presumably is a result of the higher vacuum of the Auger spectrometer, where free ligand is lost to vacuum. Traces of N that were found accounted for less than 2% of the original nitrogen content. The largest peak is associated with carbon on the surface, which is due to atmospheric contamination of the sample. The absence of detectable amounts of phosphorus on the surface is consistent with loss of all PEt_3 and the observed carbon arising from contamination.[37] Cleaning the surface by sputtering with Ar resulted in the removal of the surface layer and the observation of signals due to metallic nickel. The surface analysis is consistent with loss of all ligands from the coordination sphere resulting in the formation of highly reactive Ni. The surface layer then scavenges oxygen upon exposure to air. (See Scheme I.)

The thickness of a surface film of Ni produced from a spin-coated sample of *trans*-$(Et_3P)_2Ni(N_3)_2$ was measured by optical interferometry by comparison with an area masked with adhesive tape during the spin-coating. The mask was removed and the chip photolyzed, resulting in a step in height between the nickel film and the silicon chip. The step due to the nickel film was found to be 60 nm thick and showed no discernible variation in thickness near the step site (~0.5 mm).

(26) Ferraudi, G.; Endicott, J. F. *J. Chem. Soc., Chem. Commun.* **1973**, 674.
(27) Natarajan, P.; Adamson, A. W. *J. Am. Chem. Soc.* **1971**, *93*, 5599.
(28) Scandola, F.; Traverso, O.; Carassiti, V. *Mol. Photochem.* **1969**, *1*, 11.
(29) Knoll, H.; Stich, R.; Hennig, H.; Stufkens, D. J. *Inorg. Chim. Acta* **1990**, *178*, 71 and references therein.
(30) Klein, H.-F.; Haller, S.; Konig, H.; Dartiguenave, M.; Dartiguenave, Y.; Menu, M.-J. *J. Am. Chem. Soc.* **1991**, *113*, 4673.
(31) McGarvey, J. J.; Wilson, J. *J. Am. Chem. Soc.* **1975**, *97*, 2531.
(32) Attempts were made to prepare this complex in solution via LMCT irradiation of an acetone solution of *trans*-$(Et_3P)_2Ni(N_3)_2$. This resulted in the loss of starting material and no production of species containing coordinated azide as monitored by FTIR spectroscopy. Similar results were obtained in hexane.
(33) Beck, W.; Fehlhammer, W. P.; Pollmann, P.; Tobias, R. S. *Inorg. Chim. Acta* **1968**, *2*, 467.
(34) Hennig, H.; Stich, R.; Knoll, H.; Rehorek, D. *Z. Anorg. Allg. Chem.* **1989**, *576*, 139.
(35) Note that $^{15}N^{14}N$ is expected to have a very low extinction coefficient and has not been observed in the IR region: Pinchas, S.; Laulicht, I. *Infrared Spectra of Labelled Compounds*; Academic Press: London, 1971.
(36) Tian, R.; Facelli, J. C.; Michel, J. *J. Phys. Chem.* **1988**, *92*, 4073.
(37) Dupuy, C. G.; Beach, D. B.; Hurst, J. E., Jr.; Jasinski, J. M. *Chem. Mater.* **1989**, *1*, 16.

Scheme I

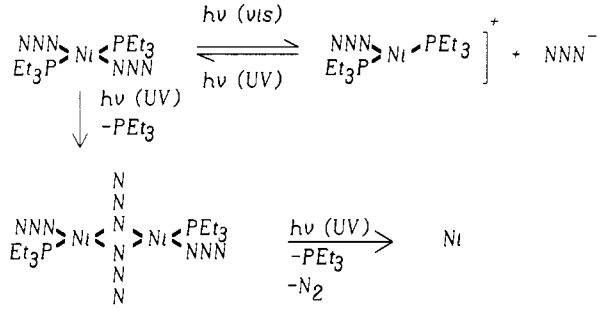

Conclusions

The results of photolysis under different conditions are summarized in Scheme I. The key points are that, as in our previous study, the photochemistry in a low-temperature glass, in this case not observable, and that in a film differ significantly. In a film, loss of all ligands may be induced photochemically at temperatures as low as 20 K. Here we have demonstrated that Ni films may be formed in a photochemical process at temperatures of 20 K.

Acknowledgment. We wish to thank B. Heinrich and K. Myrtle of the Surface Physics Laboratory, SFU, for the X-ray photoelectron spectra and Teresa W. H. Ho for preliminary experiments. We thank the NSERC (Canada) for financial support.

Appendix

The quantum yield for reaction, Φ, is given by eq A-I and is assumed to be a constant independent of the extent of reaction.

$$\Phi = -d(\textit{trans}\text{-}(Et_3P)_2Ni(N_3)_2)/d(h\nu) \qquad \text{(A-I)}$$

We may change variables at this point, substituting the mole fraction of *trans*-$(Et_3P)_2Ni(N_3)_2$, X, which will introduce a constant c, into eq A-II. Since we are irradiating with a constant

$$c\Phi = -d(X)/d(h\nu) \qquad \text{(A-II)}$$

intensity light source, the light absorbed by starting material, $d(h\nu)/dt$, will be given by A-III, where I is the intensity of the

$$d(h\nu)/dt = I[(XA'(0))/(XA'(0) + (1-X)A'(f))][1 - \exp(-(XA'(0) + (1-X)A'(f)))] \qquad \text{(A-III)}$$

incident light and $A'(0)$ and $A'(f)$ are the initial and final absorbances of the film at the irradiation wavelength.

Since we have a thin film with a low overall absorbance, we may approximate $[1-\exp(-(XA'(0) + (1-X)A'(f)))]$ as $(XA'(0) + (1-X)A'(f))$. This expression is then substituted into (A-II) (through $d(h\nu)$) which leaves a differential equation in X and t, eq A-IV, where all constants have been incorporated into the quantum yield term to give a corrected constant ϕ.

$$dX/X = \phi dt \qquad \text{(A-IV)}$$

Integration of (A-IV) followed by conversion of the mole fraction into absorbance in the IR spectrum at the monitored wavelength yields (A-V) where $A(t)$, $A(0)$, and $A(f)$ are the absorbance at the monitoring wavelength as a function of time and the initial and final absorbances, respectively. Hence, if the photoproduct does not absorb, $A(f)$ is zero and a plot of $\ln [A(t)/A(0)]$ vs time should be linear. If the product absorbs, the more general form, eq A-V, will be required to fit the data.

$$\ln [(A(0) - A(f))/(A(t) - A(f))] = \phi t \qquad \text{(A-V)}$$

Supplementary Material Available: Tables of X-ray data collection parameters, atomic coordinates and isotropic temperature factors for hydrogen atoms, and anisotropic thermal parameters for non-hydrogen atoms (2 pages); listings of structure factors and the results of the Bijvoet analysis (10 pages). Ordering information is given on any current masthead page.